LANGMUIR Article
Cite This: Langmuir 2019, 35, 12100−12112 pubs.acs.org/Langmuir

# Application of the Diffused Double Layer Theory to Nanobubbles

Jay N. Meegoda,* Shaini Aluthgun Hewage, and Janitha H. Batagoda

Department of Civil & Environmental Engineering, New Jersey Institute of Technology, 323 Dr M.L.K. Jr. Blvd., Newark, New Jersey 07102, United States

Supporting Information

**ABSTRACT:** Nanobubbles have electrically charged interfaces; hence, the diffused double layer theory can be applied to explain the behavior of nanobubbles in different electrolytic solutions. In this research, oxygen nanobubbles were generated in NaCl solutions of different concentrations, and bubble size and ζ potentials were measured just after the generation and after 1 week. The measured data and diffused double layer theory were used to compute the surface charge density, the potential due to the surface charge, and the interaction energy between bubbles. With the increased NaCl concentration, bubble size, surface charge density, and the number of negative charges increased, while the magnitude of ζ potential/surface potential, double layer thickness, internal pressure, and the electrostatic repulsion force decreased. The same trend was observed after 1 week. The net total energy calculation for the 0.001 M NaCl solution showed that the bubble repulsion for an intermediate separation distance had a $6.99 \times 10^{-20}$ J energy barrier, which prevented bubble coalescence. Hence, the 0.001 M NaCl solution produced stable nanobubbles. The calculation of internal pressure inside nanobubbles showed a reduction in the interfacial pressure difference with the increased NaCl concentration. The test results, as well as diffuse double layer and net total energy calculations, showed that the most stable bubbles were obtained with 0.001 M NaCl concentration and the least stability was recorded with the highest amount (0.1 M) of NaCl concentration.

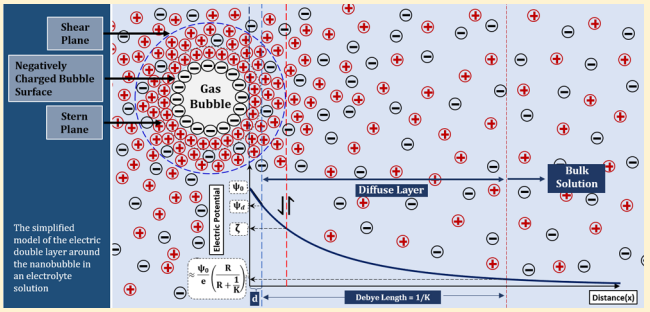


## INTRODUCTION

Nano or ultrafine bubbles are defined as gas cavities within aqueous solutions with sizes smaller than 200 nm.[1−4] In this manuscript, the bubble size refers to the bubble diameter. Nirmalkar et al.[4] experimentally proved that bulk nanobubbles do exist, they are filled with gas, and they survive for a long period of time. The industrial application of nanobubble technology has exponentially increased over the last two decades due to their long-term stability.[5,6] The extra small size, high internal pressure, and electrically charged interface are major reasons for increased industrial applications, where the bulk solution chemistry plays a significant role in nanobubbles behavior.[3] Also, smaller bubbles with low rising velocities and high ζ potential values prevented bubble coalescence.[5,7,8] Also smaller bubbles with the low buoyancy force and low raising velocities are impacted by the Brownian motion in the water molecules.[7,9,10] The stability of any colloidal system depends on two types of surface forces; electrostatic repulsion and van der Waals attraction. Hence, the Derjaguin, Landau, Verwey, and Overbeek (DLVO) theory can be used to explain the colloidal stability. The lifespan of a bubble depends on both the rising velocity[5,7,8] and gas dissolution/diffusion to the bulk solution.[11,12] The gas dissolution/diffusion depends on several factors such as gas solubility, temperature, bubble size, the pressure difference at the gas−liquid interface, interfacial reactions, and the gas saturation in the bulk liquid solution.[13] Gases within the bubble dissolve or diffuse to the bulk solution at a faster rate with higher internal pressure in the bubble.[11,12] Also, bubbles exist as clusters with an increased gas concentration within the solution and slowing the gas diffusion/dissipation from individual bubbles.[14]

The Young−Laplace equation is found to be valid at the nanoscale.[15] However, to account for the electrostatic repulsion on the surface of a nanobubble due to surface charge, Bunkin et al.[16] proposed a modification to the Young−Laplace equation. Bunkin et al.[16] showed that the pressure induced by the electric charge ($P_e$) on a nanobubble is based on the "bubstons problem" within the Coulomb model as $P_e = \frac{2\pi\sigma^2}{D\varepsilon_0}$, and hence, the modified Young−Laplace equation was expressed as shown below. (Supporting Information provides the detail derivation of the eq 1.)

$$\Delta P = \frac{2\gamma}{R} - \frac{2\pi\sigma^2}{D\varepsilon_0} \quad (1)$$

where $\gamma$ is the surface tension (N/m), $\sigma$ is the surface charge density (C/m$^2$), $D$ is the dielectric constant of the bulk liquid media, $\varepsilon_0$ is the permittivity of vacuum (C$^2$ J$^{-1}$ m$^{-1}$), and $R$ is the bubble radius (m).

Received: May 15, 2019
Revised: August 19, 2019
Published: August 21, 2019






DOI: 10.1021/acs.langmuir.9b01443
Langmuir 2019, 35, 12100−12112

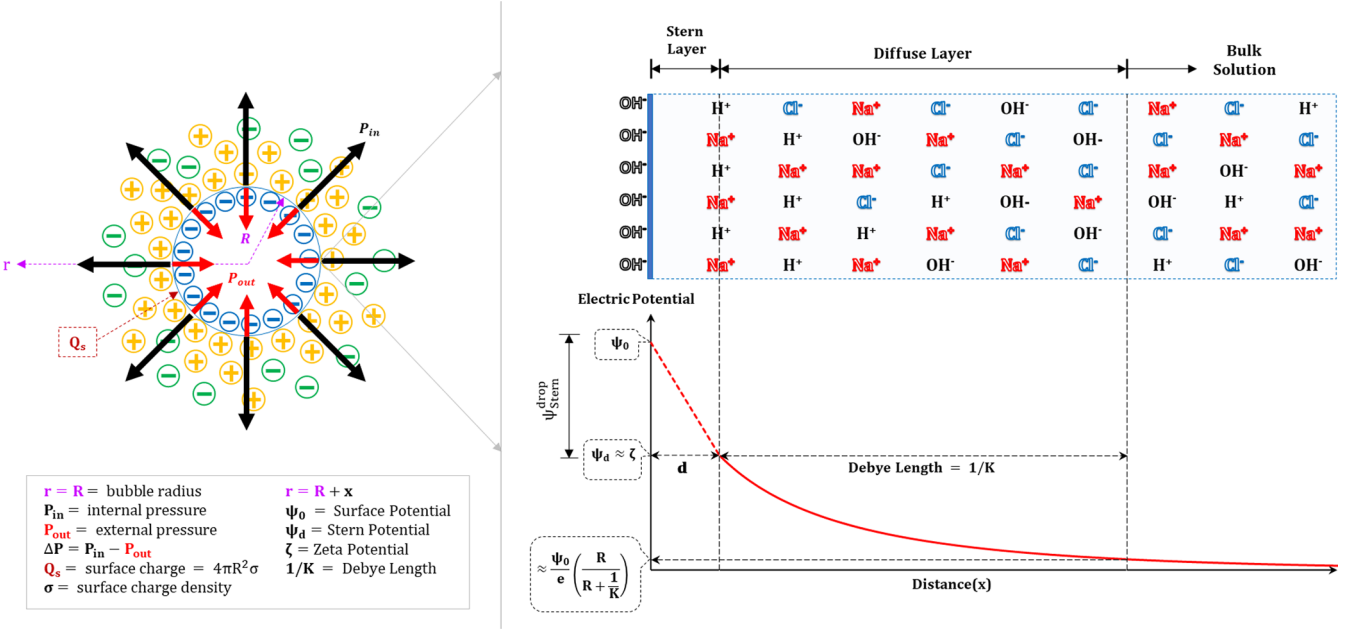


**Figure 1.** Schematic of the diffused electrical double layer formed around a nanobubble.

The accumulated ions around the bubble surface create a thin film, which acts as a diffusion barrier reducing gas dissolution, thereby increasing the lifespan of the nanobubbles and this phenomenon referred to as an ion shielding effect.[17,18]

There are many advantageous of computing double layer thickness and developing a theory to compute the electrical charges on the bubble surface, as those will provide insights to understand the physical behavior of nanobubbles in an aqueous solution. The bubble solution properties impact the bubble stability, specifically the temperature, pH, ion concentration, and dielectric constant. Thus, by changing the bulk solution chemistry, one would be able to calculate the ion distribution within the solution and, hence, the properties of nanobubbles.

Therefore, in this manuscript, the diffused double layer theory is applied to nanobubbles in an electrolytic solution using experimental data and theoretical calculations. There are different methods for nanobubbles generation: hydrodynamic cavitation, sonication causing acoustic cavitation, electrochemical cavitation, and mechanical agitation.[19] The hydrodynamic cavitation is one of the most frequently used technology. Hence, in this research, hydrodynamic cavitation is used to generate nanobubbles.

## FORMATION OF THE DIFFUSE DOUBLE LAYER AROUND NANOBUBBLES

Nanobubbles in aqueous solutions have electrically charge interfaces. This surface charge generates an electrical field that affects the ion distribution in the bulk solution. Adjacent to the bubble surface, there is a high concentration of oppositely charged ions with a diffused distribution of ions whose distance from the nanobubble neutralizes the electrical charge on the surface of the bubble. Because of the surface charge on the bubbles and the distribution of ions in the liquid adjacent to the nanobubbles, a diffused double layer formed, as shown in Figure 1. The assumptions made for the calculations of diffuse double layer parameters are discussed below.

The electric double layer consists of two layers, the Stern layer, and the diffused layer. The innermost region surrounding the bubble surface is called the Stern layer and, in this region, ions are strongly attached to the bubble surface. The next region is called the diffused layer where ions are loosely attached. In the diffused layer, there is an imaginary boundary where ions within this boundary move with the bubble, and those ions outside this boundary will not move with the bubble. This boundary is called the slip plane, and the potential at this boundary is known as the $\zeta$ potential.[20] However, the exact location of this shear plane is not well established, and there is no valid theory to calculate the shear layer thickness.[21−24] However, the $\zeta$ potential is a very important parameter for real systems as it is difficult to measure the surface potential. Though the $\zeta$ potential is not a direct measurement, it is based on the electrostatic mobility of the colloidal particles, and hence, it can be calculated. The $\zeta$ potential is commonly used to describe the stability of nanobubbles because the strong electrostatic repulsion can prevent the bubble coalescence. The $\zeta$ potential depends on the pH of the medium, the ionic strength, the concentration of any additives, and temperature. In an electrolyte solution, the double layer thickness is defined as the Debye length $1/K$ (eq S9), which is a function of the ionic strength and only depends on the properties of the solution (i.e., ionic valency, temperature, and the ion concentration in the bulk solution) and not on any property of the charged surface. Therefore, solutions with higher ionic strengths would yield a thinner double layer thickness as well as lower $\zeta$ potential value, which leads to lower repulsion, hence, increased bubble coalescence.

The Stern layer is the surface of the region between the surface of the bubbles and the locus of the hydrated counterions at a distance $d$ from the bubble surface.[25] The potential, at a distance $d$ from the bubble surface, is called the Stern potential $c$; it is the potential at the beginning of the double layer. The Stern layer thickness of clay, silica, and other colloidal surfaces are reported in the literature, but there is limited information on that of nanobubbles. Leroy et al.[26] stated that there is no Stern layer for nanobubbles. Verwey and Overbeek[27] stated that the Stern layer in a clay−water electrolyte system is approximately 0.5 nm.[28] Shang et al.[29] stated that, for the clay−water electrolyte system, the Stern layer thickness is two monomolecular layers of



DOI: 10.1021/acs.langmuir.9b01443
Langmuir 2019, 35, 12100−12112

adsorbed water, where $d$ varies between 0.5 and 0.6 nm.[29] Sridharan and Satyamurty[30] stated that the Stern layer thickness is equal to the hydrated exchangeable cationic radius. Brown et al.[31] showed that the Stern layer thickness is always one hydrated cation radius plus one molecule layer of water (2.1−2.7 Å) and concluded that cations are absorbed via nonspecific interactions with silica particles. Herbowski et al.[32] stated that the Stern layer consists of mostly ions; hence, its thickness is on the order of 0.2 nm because it depends on the diameter of ions. The $K^+$, $Na^+$, and $Cl^-$ ions have radii of 0.125, 0.183, and 0.1206 nm, respectively.[32,33] Lim et al.,[34] on the basis of the Nernst−Planck−Poisson equations, reported that the Stern layer thickness is equal to 0.5 nm (slightly larger than one hydrated ion radius).

Even though there is no experimental evidence on the Stern layer of nanobubbles, since the bubbles are electrically charged, a diffuse double layer is formed around the bubble surface. In this research, the thickness of the Stern layer is assumed as equal one hydrated ion radius. This is due to no firmly attached water molecule layer, unlike in clay/silica particles.

In this study, NaCl is used as the electrolyte solution, the hydrated Na ion radius of 4.7 Å (0.47 nm) was assumed as the $d$ value.[35,36] The $\zeta$ potential is equal to or lower than the magnitude of Stern potential ($|\zeta| \leq |\psi_d|$). The difference between $\psi_d$ and $\zeta$ is a function of the ionic strength; at low ionic strength, the decay of the potential as a function of distance is small and $\zeta \cong \psi_d$; at high ionic strength, the decay is steeper and $|\zeta| \leq |\psi_d|$.[32] As mentioned before, the accurate position of the shear plane is unknown, and over past decades the position of the shear plane has become a subject of great interest for many researchers.[22,26] One of the common general assumptions in the literature is that the shear plane is roughly equal to the Stern plane.[22,24] However, a few researchers are of the opinion that the shear plane is located far away from the Stern plane but close to the Gouy plane (the Debye−Hückel length, $1/K$).[24] Liu et al.[21] showed that the position of the shear plane depends on the polarization of counterions and concluded that, with ion polarization, there is a higher reduction in the Stern potential than that at the Gouy plane and the thickness of shear plane deceased with increased polarization. In this research, the $\zeta$ potential is assumed to equal to the Stern potential ($\zeta \cong \psi_d$). Hence, the surface potential can be expressed as

$$\psi_0 = \psi_{\text{Stern}}^{\text{drop}} + \zeta \tag{2}$$

where the Stern layer can be assumed to act as a parallel concentric sphere capacitor[27] and the potential drop is assumed to be linear within the Stern layer. Hence, $\psi_{\text{Stern}}^{\text{drop}}$ is

$$\psi_{\text{Stern}}^{\text{drop}} = \sigma_0\left(\frac{d_{\text{Stern}}}{\varepsilon\varepsilon_0}\right) \tag{3}$$

by assuming the highest potential value of the diffuse layer potential is equal to the $\zeta$ potential, for the electroneutrality of $\sigma_0 = -\sigma_D$, where $\sigma_0$ is the surface charge density and $\sigma_D$ is the excess charge density in the diffuse layer.

## DERIVATION OF SURFACE CHARGE DENSITY EQUATIONS

The Poisson−Boltzmann equation was used to describe the distribution of ions around the charged particle. The derivation of the Poisson−Boltzmann equation for spherical geometry with 1:1 electrolyte solution is shown in Supporting Information eqs S5−S7. By solving the Poisson−Boltzmann equation, we can calculate the electric potential, $\psi(x)$, around the sphere.

Now consider a bubble of radius $a$ having a surface charge density of $\sigma$ or the total charge $Q$ ($=4\pi a^2\sigma$) and the net charge density $\rho(r)$ at a distance $r$ from the center of the sphere, so that the total surface charge density is shown in eq 4 (simplifications are shown in the Supporting Information eqs S11−S13).

$$\therefore \sigma = \frac{1}{a^2}\int_{r=\infty}^{r=a} \rho(r) r^2 \, dr \tag{4}$$

The double layer must be electrically neutral; therefore, the total charge on the bubble surface ($\sigma_0$) must be equal and opposite in sign to the net charge density of the diffused layer ($\sigma_D$). Hence, by simplifying the Boltzmann equation (eq S5) and potential distribution eqs (eq S8 or eq S10), we can calculate the net charge density ($\sigma_D$).

Debye and Hückel[37] proposed a potential distribution eq (eq S8), and the net charge density ($\sigma_D$) can be expressed as

$$\begin{aligned}\sigma_D &= \frac{-2Zq\rho_{\text{bulk}}}{a^2}\int_{x=\infty}^{x=0} \sinh\left(\frac{Zq}{kT}\psi_d\left(\frac{a}{a+x}\right)\exp(-Kx)\right) \\ &\quad \times (a+x)^2 \, dx \\ &= -\sigma_0\end{aligned} \tag{5}$$

Similarly, Tuinier[38] proposed the potential distribution equation, where the net charge density ($\sigma_D$) can be expressed as

$$\begin{aligned}\sigma_D &= \frac{-2Zq\rho_{\text{bulk}}}{a^2}\int_{x=0}^{x=\infty} \sinh\left[\frac{Zq}{kT}\left(\left(\frac{2a}{a+x}\right)\right.\right. \\ &\quad \times \ln\left(\frac{1+t_0\exp(-x)}{1-t_0\exp(-x)}\right)[1-\exp(-0.3a)] \\ &\quad \left.\left. + 2\ln\left(\frac{1+u_0(x)\exp(-x)}{1-u_0(x)\exp(-x)}\right)[\exp(-0.3a)]\right)\right](a+x)^2 \, dx \\ &= -\sigma_0\end{aligned} \tag{6}$$

Equations 5 and 6 can be numerically integrated to generate tables that can be easily modified by including input parameters and constants to obtain the surface charge density as output. Numerical integrations are performed using the Trapezoidal Rule (Supporting Information eq S16), and by having small intervals of distances to generate accurate results.

Although numerical analysis has an ability to provide accurate results, approximate analytical solutions are still valuable as they can be conveniently applied with tolerances. Therefore, in this research, two approximate analytical solutions for the surface charge density $\sigma_0$ of the particle were derived for 1:1 electrolyte solution. The two approximate analytical solutions derived by Loeb et al.[39] and Ohshima et al.[40] are shown in eqs 7 and 8, respectively (simplifications are shown in Supporting Information eqs S17−S21).

$$\sigma_0 = \frac{\varepsilon_r\varepsilon_0 KkT}{q}\left[2\sinh\left(\frac{q\psi_0}{2kT}\right) + \frac{4}{Ka}\tanh\left(\frac{q\psi_0}{4kT}\right)\right] \tag{7}$$



DOI: 10.1021/acs.langmuir.9b01443
Langmuir 2019, 35, 12100−12112

$$\sigma_0 = \frac{\varepsilon_r \varepsilon_0 KkT}{q}\left[2\sinh\left(\frac{q\psi_0}{2kT}\right)\right] \times \left[1 + \frac{2}{Ka\cosh^2\left(\frac{q\psi_0}{4kT}\right)} + \frac{8\ln\left[\cosh\left(\frac{q\psi_0}{4kT}\right)\right]}{(Ka)^2\sinh^2\left(\frac{q\psi_0}{2kT}\right)}\right]^{1/2} \quad (8)$$

## INTERFACIAL FORCES

In 1940 the DLVO theory was separately developed by Derjaguin, Landau, Verwey, and Overbeek, to explain the stability of colloids by considering the balance between the attractive, short-range van der Waals forces, and the repulsive electric double layer forces.[41,42]

In the case of nanobubbles, with the electrically charged interface, the overlap of the interacting double layers produces electrostatic repulsion due to the increased counterions between the bubbles (i.e., consider interacting bubbles with similar charges (sign negative/positive)). Also, with similar size bubbles, there is an attractive force due to the dipole−dipole interactions, known as van der Waals forces.

The bubble−bubble interaction can be considered in two ways. First by considering the stability due to force equilibrium and the second by computing the potential for bubble collision. In order to explore the bubble stability (the possibility of coalescence, repulsion or no net force), the repulsive and attractive forces were calculated using experimental data (i.e., size and $\zeta$ potential). Here an assumption is made that the calculated surface potentials remain constant for all bubble separation distances. Then the resultant force is calculated for different solution concentrations. Here a quantitative analysis of the bubble dynamics was not be performed (i.e., the bubble approaching speed/collision rate), which is the second approach, the bubble collision. Such computation is complex and requires the consideration of bubble deformation, the ions regulation phenomenon (ion rearrangement and nonuniform surface charge densities) as bubbles approach each other, the size of the bubble, the change in of bubble size over time due to the gas diffusion, and the induced bubble movement due to Brownian motion.

For droplet coalescence calculations, the droplet deformation and the thin liquid film between droplets are accounted for.[43,44] However, for nanobubbles with high internal pressures, bubbles are rigid with limited deformation, and hence, they maintain a spherical shape. Chen et al.[45] stated that the deformation of microscale droplets could be safely disregarded for oil droplets smaller than 10 $\mu$m. Hence, in this study, for the calculation of both the van der Waals forces and the electrostatic repulsive forces, nanobubbles are assumed as perfect spheres for all separation distances. Moreover, until the moment of bubble collision, the assumption of the spherical shape should not introduce errors to the calculations. Accordingly, the resultant net energy ($W(D)$), and net force ($F = \mathrm{d}W/\mathrm{d}D$), as well as van der Waals attractive energy/force and double layer repulsive energy/force versus separation distances ($D$) can be plotted for two identical spherical nanobubbles. The classical equations used in this research were obtained from the literature and described in detail in the enclosed Supporting Information. For the small separation distance ($D \ll R$), the total energy is given by

$$W(D) = \frac{-A}{6D}\left(\frac{R_1R_2}{R_1 + R_2}\right) + K\left(\frac{R_1R_2}{R_1 + R_2}\right)Ze^{-kD} \quad (9)$$

where $A$ is the Hamaker constant, $R_1$ and $R_2$ are the radii of each spherical particle whose interacts each other, $D$ is the separation distance, $K^{-1}$ is the Debye length, $Z = 64\pi\varepsilon_0\varepsilon(kT/e)^2\tanh^2(ze\psi_0/4kT)$, and for this study, $R_1 = R_2$ and $A = 4.05 \times 10^{-20}$ J (the detailed calculation of the Hamaker constant is also included in the enclosed Supporting Information).

## MATERIALS AND METHODS

To generate nanobubbles, a 25 L container was used and filled up to 18 L. Nanobubbles were generated using the hydrodynamic cavitation method.[46−49] A BT-50FR micronano sized nozzle[46,50,51] with 55 psi capacity water pump was used to generate nanobubbles. To generate nanobubbles, water was allowed to flow through the nanobubbles generating a nozzle for 3 min, while supplying oxygen gas. In this experiment, oxygen nanobubbles were generated using compressed oxygen in a cylinder with a regulator.

After the generation of nanobubbles, samples were collected and tested to obtain bubble size distribution and $\zeta$ potential values of using the Malvern Zetasizer Nano ZS.[52−54] The Zetasizer measures the size of the particles using the technique called dynamic light scattering (DLS), which measures the Brownian motion of the particles and relates this to the size of the particles using the Stokes−Einstein equation.[55] Brownian motion is measured by illuminating the particles with a laser and analyzing the fluctuation in scattering intensity. The Zetasizer is based on the noninvasive back-scatter (NIBS) system, which increases the accuracy of the measurements compared to conventional optics. The Zetasizer analyzes the $\zeta$ potential by determining the electrophoretic mobility of the particles and then applying Henry's equation based on the Smoluchowisk's approximation/model. The majority of published literature on nanobubbles used the Smoluchowiski's model to calculate the $\zeta$ potential.[5,52−54]

Schnitzer et al.[56] showed that the behaviors of solid particles and the bubbles/droplets are different at the interface of the particle/bubble and the liquid. The solid−liquid interface is considered as rigid with the no-slip, while the liquid−liquid or gas−liquid interface should be considered a mobile interface. Hence, Schnitzer et al.[56] concluded that Smoluchowiski's model in the field-driven motion of drops and bubbles with mobile interfaces is not applicable. However, their analysis was limited to the ordinary bubbles/droplets and not for nanobubbles. Also the nanomechanics is quite different from that of micro or macromechanics. Nanobubbles have high internal pressure and, hence, are rigid with insignificant deformations. Furthermore, the nanobubbles are stable and long-lasting, hence, minimal dissolution or diffusion, due to extraordinary interfacial characteristics when compared to ordinary bubbles. Also one of the hypotheses of nanobubbles stability is the accumulated ions limiting the gas diffusion due to the ion shielding effect.[17,18] Also the nanobubbles interfacial characteristics were examined by Nakashima et al.[57] and Ohgaki et al.,[58] who explained that the characteristics of the interfacial film and the interface of nanobubbles consisted of highly structured hydrogen bonds. Therefore, on the basis of the aforementioned, it assumed that nanobubbles have rigid interfaces with high internal pressures and resistance to the diffusion and dissolution and, hence, behave fundamentally different from that of ordinary bubbles. Therefore, it was assumed that Smoluchowisk's approximation could be used without significant error.

Electrophoretic light scattering (ELS) is a technique used by the Zetasizer to measure the electrophoretic mobility of the particles in dispersion; this technique is based on the electrophoresis. In this research, the measurements were taken using the folded capillary cell (DTS1070) for both the size and the $\zeta$ potential, where the cell contains two electrodes. Once the electrical field is applied to the electrodes,



DOI: 10.1021/acs.langmuir.9b01443
Langmuir 2019, 35, 12100−12112

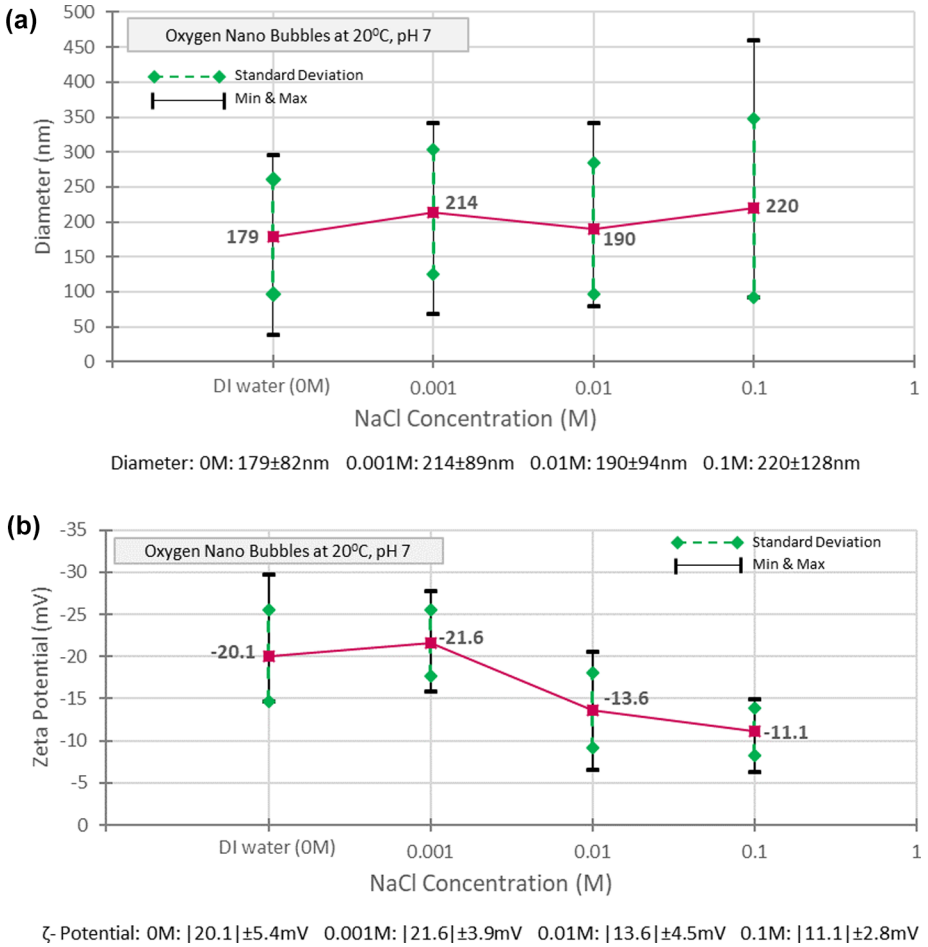


**Figure 2.** Relationship between NaCl concentration and (a) bubble diameter and (b) $\zeta$ potential, for oxygen nanobubbles at 20 °C and pH ≈ 7.

bubbles that have a net charge, or a $\zeta$ potential will travel toward the oppositely charged electrode and the velocity of this mobility/movement is measured based on the laser doppler velocimetry (VDL) technique combined with M3-PALS technology. This method used the mixed-mode measuring techniques that allowed us to measure the $\zeta$ potential without the influence of electrical osmosis. The mixed-mode measurement is the method of changing the reversal cycle of the electric field, which is fast-field-reverse (FFR) and slow-field-reverse (SFR).[49]

All experiments were carefully conducted to avoid possible contamination. Before the bubble generation, water was tested for the presence of any nanosize material using the Zetasizer. Always the system was cleaned/washed out before each test. In this research, deionized (DI) water and different NaCl concentrations (0.001, 0.01, and 0.1M) were prepared. Freshly collected DI water was collected in a 100 L tank and allowed to come to equilibrium with the atmospheric gases at the room temperature for 24 h. Prior to the generation of nanobubbles, the gas concentrations in the bulk water in contact with air at 25 °C were as follows: oxygen, −8.72 mg/L (and at 22 °C, oxygen, −9.2 mg/L); nitrogen, −13.34 mg/L; carbon dioxide, −0.5 mg/L; negligible amounts of other gases in the air. For each test the same bulk liquid was used, the appropriate amount of salt was added, and allowed to be in equilibrium with air. Then these solutions were used to create oxygen nanobubbles. Generated nanobubbles were tested immediately after generation and 7 days after generation.

## RESULTS AND DISCUSSION

Figure 2a shows the variation of bubble sizes and Figure 2b shows the variation of $\zeta$ potential values of the oxygen bubbles in different solutions of NaCl concentrations. Figure 3 shows the same test results just after the bubble generation (week 0) and after 1 week of generation (week 1). The size/diameter results were recorded as the number-distribution data, where the peak values of the distribution curves are reported.

Reported test results in Figures 2 and 3 show the minimum, maximum, and average values as well as the standard deviation values based on six measurements for each test with different salt concentrations. The results show that with the increase in NaCl concentration, the bubble diameter slightly increased, and the magnitude of $\zeta$ potential decreased. All measured $\zeta$ potential values were negative. Hence, from here onward $\zeta$ potential values are reported without their sign. Figure 3a shows the variation of bubble diameter with time for different concentrations of NaCl solutions, where bubble diameter increased with time for all solutions. Figure 3b shows the variation of $\zeta$ potential values with time for different concentrations of NaCl solutions, where with time $\zeta$ potential values decreased.

The measured data are used to compute the surface charge density, surface potential, double layer thickness, and internal gas pressure inside nanobubbles. Table 1 shows all the measured data as well as calculations for both week 0 and week 1. Columns 1, 2, and 3 show the NaCl concentration, bubble size, and the $\zeta$ potential values, respectively. Column 4 shows the calculated double layer thickness ($1/K$) based on the eq S9. For the DI water bubble solution, there is no Stern layer without salts. Hence, the double layer thickness was not computed for the DI water bubble solution. Column 5 shows the calculated surface charge density for each test. The calculated surface charge


DOI: 10.1021/acs.langmuir.9b01443
Langmuir 2019, 35, 12100−12112

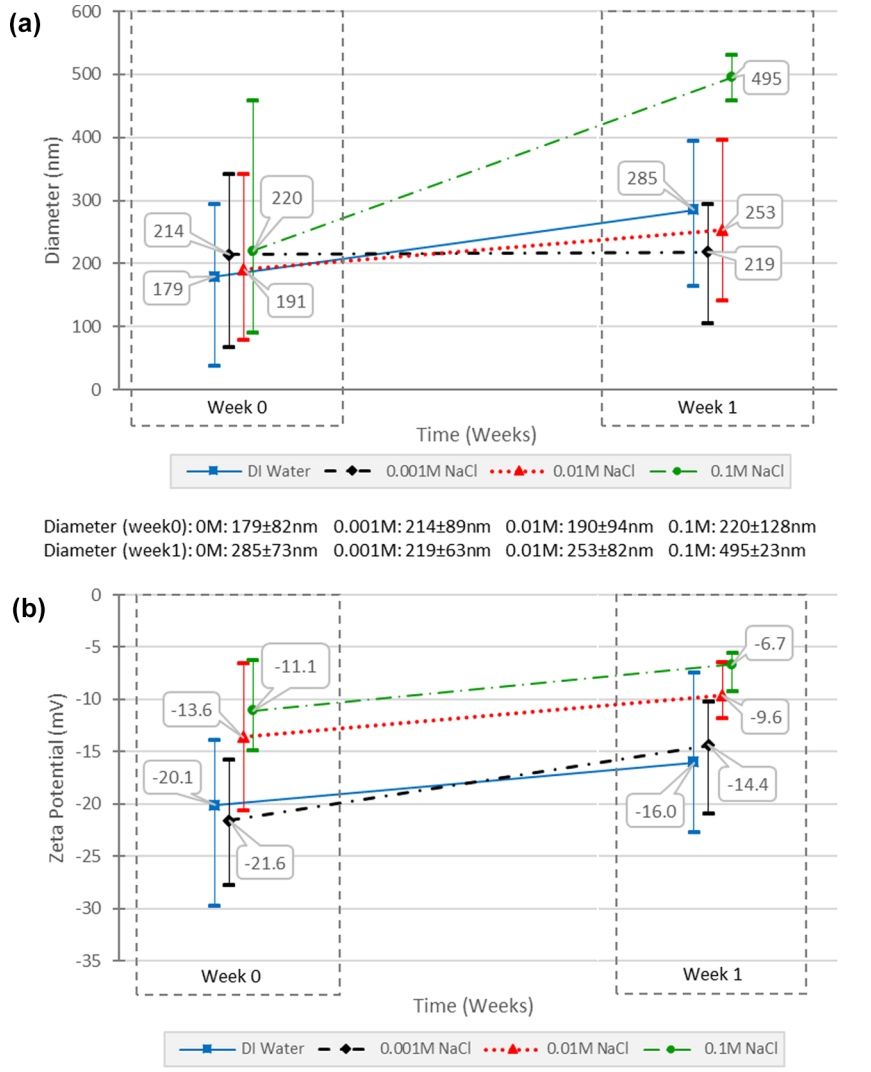


**Figure 3.** Variation with time of (a) diameter and (b) $\zeta$ potential, for oxygen nanobubbles in NaCl solution at 20 °C and pH ≈ 7.

densities were based on the numerical and analytical solutions (obtained same results) presented in eqs 5, 6, 7, and 8. Column 6 shows calculated surface potentials, $\psi_0$ for each test. Surface potential values were calculated based on eqs 2 and 3. For the electrolyte solutions, the thickness of the Stern potential ($d$) was assumed as equal to the hydrated Na ion with an effective radius of 0.47 nm as previously explained. Column 7 shows the number of negative charges on the bubble surface (negative charge = (surface charge density × surface area)/electron charge). Finally, column 8 shows the calculated pressure difference across the fluid interface ($\Delta P$) based on eq 1).

Figure 3 and Table 1 illustrate that with the increase in NaCl concentration of the solution, bubble sizes slightly increased. Also, a week after the bubble generation, for all the solutions bubble sizes increased. Furthermore, at week 0, $\zeta$ potential values decreased with the increase in NaCl concentration, and all the values (bubble size as well as $\zeta$ potential values) decreased after 1 week. For the 0.001 M salt concentration, the bubble size appears to be stable, with only a 2.3% increase in bubble size after 1 week. However, the reduction in $\zeta$ potential was comparatively high. Also, with higher concentrations of NaCl (0.01 and 0.1 M), the increase in bubble size and reduction in $\zeta$ potential values were significantly higher. The average surface charge densities and $\zeta$ potential values at week 0 and week 1 were plotted against concentrations of NaCl solutions and shown in Figure 4. Figure 4 shows that with increased NaCl concentrations, the $\zeta$ potential decreased, and the magnitude of surface charge density increased.

Figure 5 shows the distribution of electric potential with the normalized distance against bubble radius for four NaCl solutions and corresponding calculated double layer thicknesses values corresponds to the week 0 test results.

It can be clearly observed from Figure 5 that the variation of electrical potential with distance had a steep rate of decline for solutions of higher NaCl concentrations and produced thinner double layer thickness values.

Figure 6 shows the total number of negative charges on the bubble surface for week 0 and week 1. It also shows the variation in double layer thickness with increased concentrations of NaCl solutions for both week 0 and week 1. For all solutions, the double layer thickness becomes thinner after 1 week when



DOI: 10.1021/acs.langmuir.9b01443
*Langmuir* 2019, 35, 12100−12112

Table 1. NaCl Solution Concentration with Average Size, Average ζ Potential, and the Calculated double Layer Thickness, Surface Charge Density, Surface Potential, Number of Electrons, and Pressure Difference across the Fluid Interface

| col 1 | col 2 | | | col 3 | | | col 4 | | col 5 | | col 6 | | col 7 | | col 8 | |
|---|---|---|---|---|---|---|---|---|---|---|---|---|---|---|---|---|
| | diameter (nm) | | | ζ potential (mV) | | | double layer thickness (DLT/radius) | | surface charge density ($\sigma_0$) (C/m$^2$) | | surface potential ($\psi_0$) (mV) | | no. of negative charges | | av pressure ($\Delta P$) (atm) | |
| [NaCl] (M) | week 0 | week 1 | % increase | week 0 | week 1 | % reduction in magnitude | week 0 | week 1 | week 0 | week 1 | week 0 | week 1 | week 0 | week 1 | week 0 | week 1 |
| 0 | 179 | 285 | 59.2 | −20.10 | −16.00 | 20.4 | N.D. | N.D. | N.D. | N.D. | N.D. | N.D. | N.D. | N.D. | N.D | N.D |
| 0.001 | 214 | 219 | 2.3 | −21.59 | −14.38 | 33.4 | 0.090 | 0.088 | −0.0018 | −0.0012 | −22.78 | −15.15 | 1605 | 1098 | 13.0 | 12.9 |
| 0.01 | 190 | 253 | 33.2 | −13.58 | −9.63 | 29.1 | 0.032 | 0.024 | −0.0033 | −0.0023 | −15.77 | −11.16 | 2341 | 2900 | 14.0 | 10.8 |
| 0.1 | 220 | 495 | 125.0 | −11.07 | −6.66 | 39.8 | 0.009 | 0.004 | −0.0083 | −0.0049 | −16.57 | −9.94 | 7873 | 23725 | 6.9 | 3.6 |

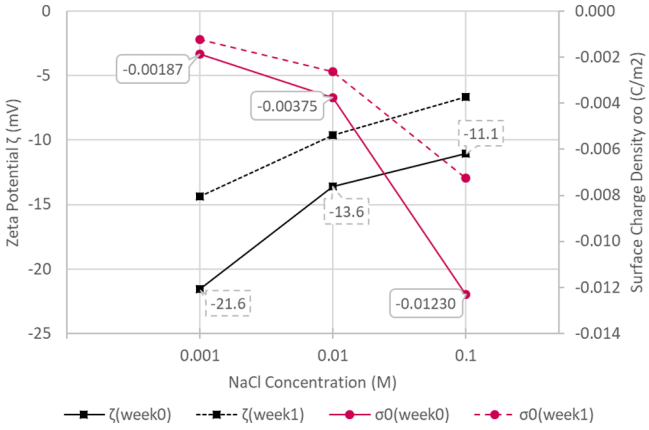


**Figure 4.** Surface charge density for oxygen nanobubbles in NaCl solution at 20 °C and pH pH ≈ 7.

compared to those for week 0 (Table 1). The double layer thickness declined with the increase in salt concentration.

For bubble solutions with lower salt concentrations, there was no substantial change in the number of negative charges on bubble surfaces after 1 week. However, at high solution salt concentrations of 0.1 M, the total number of surface charges increased to form large bubbles. To have such a high increase in the number of negative charges on the bubble surface, several bubbles should have merged to form larger bubbles. Hence, at high solution salt concentrations, nanobubbles seem to be much more vulnerable to coalescence due to the reduction in ζ potential and related thinner double layer thicknesses.

With the increase in ion concentration in the bulk solution, surface charge density increased while the absolute ζ potential/surface potential decreased due to the corresponding reduction in the diffuse layer thickness values of the nanobubbles. Even though, with the increase in NaCl concentration, a decrease in ζ potential can be attributed to the thinning of the double layer thickness, the increase of negative charge density or the total amount of negative charge is unexpected. With the hypothesis that the negative charges of the nanobubbles are absorbed $OH^-$ ions[46] at the gas−liquid interface, especially for DI solution, this result suggests that the $OH^-$ adsorption was stabilized by the added NaCl. A similar phenomenon was discussed by the Higuchi et al.[59] for polymer material in water by considering the charge regulation mechanism. By applying their finding to nanobubbles, when the two charged ions (i.e., $OH^-$) at the bubble surface approach each other, the surface charge density will be reduced to decrease the electrostatic repulsion either by absorption of the counterions and/or desorption or removal of surface charge. Therefore, it can be concluded that any increase in the ionic strength would favor the $OH^-$ absorption as the reduction in electrostatic (repulsion) energy between absorbed $OH^-$ ions.

For lower NaCl concentrations, the double layer thickness did not significantly affect the ζ potential values. For high concentration solutions (i.e., 0.01 and 0.1 M), the negative charge density and the amount of negative charge increased, and this was confirmed by calculations as well. Even though absorbed $OH^-$ density is high, with the high ionic strength the electrostatic repulsion between absorbed $OH^-$ ions have to be weakened due to the increased amount of counterion concentration and the Debye length is sufficiently short and resulted in lowering the ζ potential. In such a situation, the charge regulation mechanism may become less effective



DOI: 10.1021/acs.langmuir.9b01443
Langmuir 2019, 35, 12100−12112

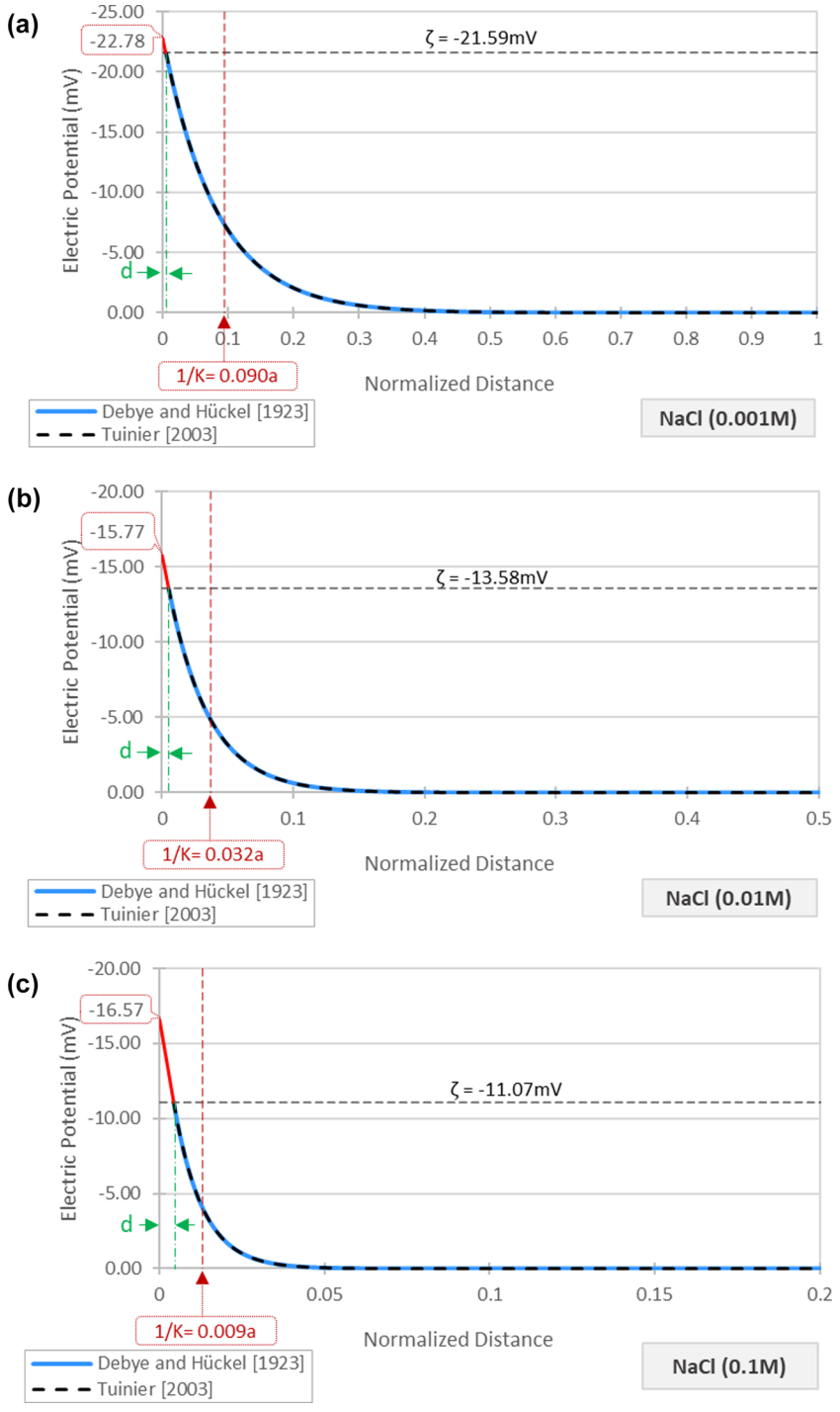


**Figure 5.** Variation of electrical potential with distance for oxygen nanobubbles in NaCl solutions of varying concentrations (20 °C and pH ≈ 7).

compared to the weakened long-range repulsion, causing the increase of the bubble coalescence.

The gas dissolution rates in a nanobubble would depend on the inside gas pressure, with higher gas pressures causing higher diffusion rates. Column 8 of Table 1 shows the variation of average gas pressure in bubbles with different concentrations of the NaCl solutions (based on eq 1). Figure 7 shows the predicted gas pressures inside nanobubbles for three salt solutions based on the Young−Laplace and the modified Young−Laplace equation. Results show that, with increased salt concentration, the pressure difference at the gas−liquid interface decreased; however, the bubble diameter did not significantly vary with the increased concentration of the NaCl solution. Even though it was expected that, with high surface charge densities, internal pressures inside the bubble would reduce, the results indicate that the contribution was minimal. Only with a high amount of NaCl (i.e., 0.1 M) was there a considerable reduction in internal gas pressure. Table 1 shows that, with the increase in surface charge density, there is minimal change in bubble characteristics as the inside gas pressure is still significantly high. Table 1 and Figure 7 show that, for nanobubbles in 0.001 M salt solution, the internal gas pressure did not significantly vary after 1 week.



DOI: 10.1021/acs.langmuir.9b01443
*Langmuir* 2019, 35, 12100−12112

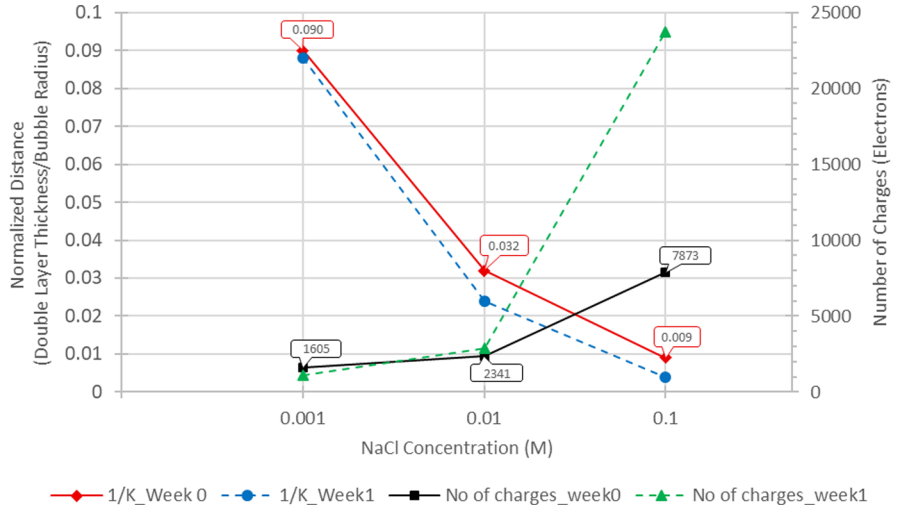


**Figure 6.** Variation of the electric double layer thickness and number of electrons with NaCl concentration for oxygen nanobubbles at 20 °C.

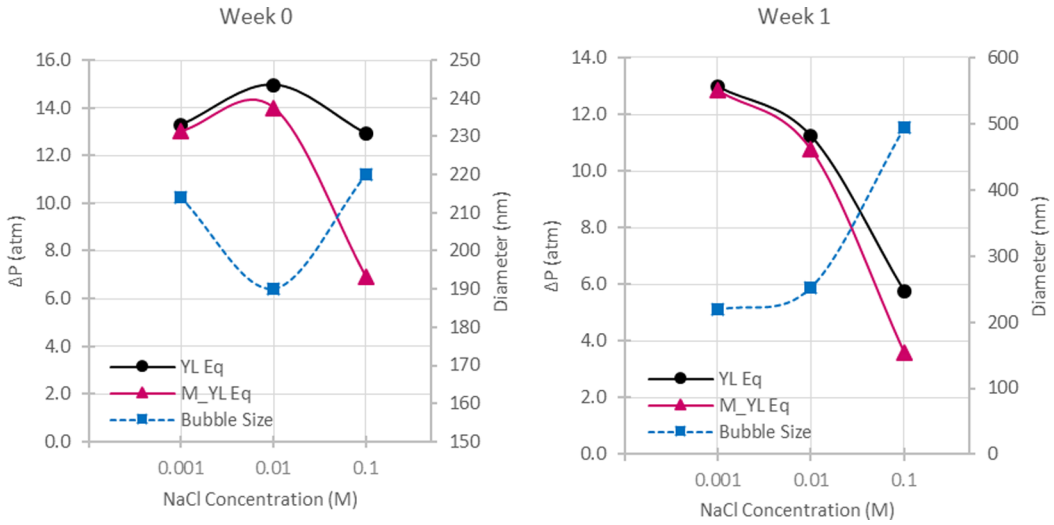


**Figure 7.** Pressure difference across the fluid interface ($\Delta P$) based on the Young–Laplace equation and modified Young–Laplace equation.

Figure 8 shows that the van der Waals energy/force, electric double layer repulsion energy/force and the total energy/force for 0.001, 0.01, and 0.1 M NaCl concentrations. For the 0.001 M NaCl solution, with higher repulsive energy/forces, a stable nanobubble solution was created as the bubble coalescence was prevented due to the neutralization of the van der Waals interactions. On the basis of Figure 8a, there is comparatively high electrostatic repulsion, and hence, the total interaction energy is positive for the intermediate separation distances. Also, there is a peak energy barrier of $6.99 \times 10^{-20}$ J with zero net interaction force for a critical separation distance of 4.92 nm. However, for higher NaCl concentration solutions (0.01 and 0.1 M), results clearly indicated that the energy barrier disappeared, and total interaction energy and forces are dominated by the van der Waals attraction. This indicates that the net energy and force curves are always attractive with high potential for bubble coalescence (Figure 8b,c). The net negative energy and attractive force are shown in Figure 8b,c and indicate that the electrostatic repulsion is very sensitive to the ionic strength of the solution.

The higher concentration of ions in the solution reduces the double layer interaction between the charged surfaces, resulting in the reduction in double layer thickness, and thereby reducing the magnitude of repulsive interaction, while the van der Waals attraction is insensitive to the electrolyte concentration. At the very smaller separation distance, the van der Waals force is always greater than the electrostatic force, because the van der Waals forces are based on the power law. This phenomenon can be seen in Figure 8a as well, where the separation distance becomes smaller, and the net interaction energy is negative for separation distances less than 1 nm, which can lead to bubble coalescence at smaller separation distances. Hence, the above observations can be summarized as, for similarly charged bubbles, at low NaCl concentration, there is high double layer repulsion preventing bubble coalescence.

On the basis of the above discussion, it can be stated that the most stable bubbles were obtained with 0.001 M NaCl concentration and the least stability was recorded with the highest amount (0.1 M) of NaCl concentration. Also, the experimental results showed that nanobubbles could be generated in DI water. This indicates that the stability of nanobubbles is a complex chemical and physical phenomenon. Therefore, there must be multiple factors contributing to the stability of nanobubbles as experimental data showed the existence of nanobubbles for long time periods. Hence, the mechanism behind the stability of nanobubbles is not just


DOI: 10.1021/acs.langmuir.9b01443
*Langmuir* 2019, 35, 12100–12112

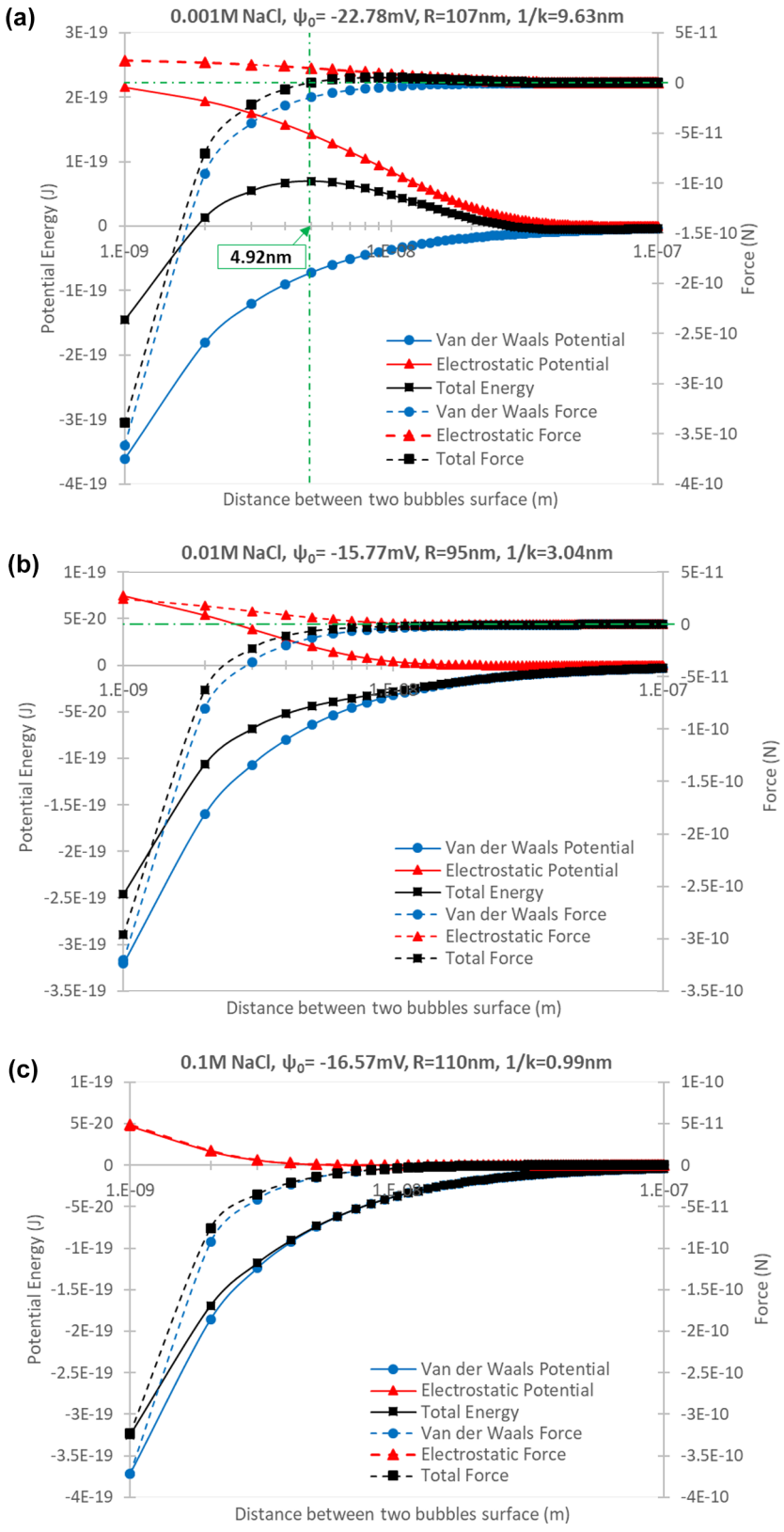


**Figure 8.** van der Waals, electrostatic and total energy and forces vs separation distances for nanobubbles in NaCl solutions for varying concentrations (20 °C, pH ≈ 7).

limited to smaller in size and having a high surface charge but a more complex phenomenon.

Dressaire et al.[17] explained that bubble stability using a diffusion barrier because of ion accumulation (ions shielding). Uchida et al.[18] used a transmission electron microscope to analyze nanobubbles and observed a thin film around the bubble surface. They speculated that this thin layer consisted of impurities (including NaCl and NaCl−2$H_2O$) and hypothe-



DOI: 10.1021/acs.langmuir.9b01443
*Langmuir* 2019, 35, 12100−12112

sized that the $Na^+$ ion accumulation in the aqueous solution reduced the gas dissolution rate. Nakashima et al.[57] and Ohgaki et al.[58] reported that apparent stability of nanobubbles would strongly depend on the characteristics of the interfacial film and the interface of nanobubbles consisted of highly structured hydrogen bonds. Seddon et al.,[60] Weijs et al.,[14] and Uchida et al.[18] reported that bubble gas dissolution rate decreased as the bubble solution become saturated with gas (diffusive shielding). On the basis of the bubble suspended solution and bubble state (undersaturated, saturated or supersaturated), bubbles can either to grow or shrink.

The behavior of smaller nanobubbles is quite complex. This is because, in addition to saturation levels, the surface tension forces play a vital role. In order to achieve thermodynamic equilibrium, the bubble system should be chemically and mechanically in equilibrium. The bubble will be mechanically stable when the total outward pressure from inside the bubble at the gas−liquid interface is equal to the total inward pressure at the gas bubble interface as expressed by eq 1. The bubble will be chemically in equilibrium when partial pressures of each gas type in the bubbles are equal to their respective bulk liquid gas pressure described by Henry's law. However, if the bulk liquid is supersaturated relative to the bubble, then there is a bulk gas movement into the bubble. Also, if the bulk medium is undersaturated, then there is bulk gas movement out of the bubble. If gas pressures are in equilibrium, the bubble size will remain unchanged, and there will be no mass transfer between the bubble and the surrounding liquid.[61] In such conditions, bubbles are considered to be either thermodynamically stable (globally lowest total free energy) or thermodynamically metastable (locally lowest total free energy, but not globally minimum free energy).[61] These metastable bubbles would eventually change to another metastable state or to a thermodynamically equilibrium state. Therefore, nanobubble stability would also depend on the gas concentrations in the solution and inside the bubble. Therefore, there is an urgent need to develop methods to accurately determine the gas concentration/pressure inside nanobubbles.

If there is nanobubble coalescence, where bubbles grow in size by merging with adjacent nanobubbles, bubble merging can be caused due to different mechanisms. The coalescence of similar size bubbles may be due to the Brownian motion, while if the bubbles are of different sizes, they can be merged due to the Ostwald ripening effects. According to Henry's law and the Gibbs−Thomson equation, the smaller sized bubbles are a source of gas in the surrounding solution.[18] Therefore, a larger bubble grows as the smaller bubble diffuses into larger bubbles. For the comprehensive investigation of nanobubbles stability, all the phenomena (i.e., surface charge, saturation level, diffusion rates, chemical potentials, surface tension, etc.) should be simultaneously considered. Such analysis is possible with the use of molecular dynamic simulations.

## CONCLUSIONS

In this manuscript, the ion distribution around the bubbles, and hence, the presence of a diffuse double layer theory was applied to nanobubbles in salt solutions of different concentrations. The surface charge density values on nanobubbles were computed using numerical simulations as well as previously developed analytical solutions. Then the double layer thicknesses, van der Waals attractive force, electrostatic repulsive force, and the net interactive energies and forces were calculated. With the increase in NaCl concentration, bubble size increased, and $\zeta$ potential/surface potential decreased. With the reduction in $\zeta$ potential values, there was a corresponding reduction in double layer thickness. The literature confirmed that, with an increase of NaCl concentration, a reduction in negative $\zeta$ potential and an increase in effective diameter.[7,62,63] Also, the surface charge density and amount of total negative charge increased, and this was explained as $OH^-$ absorption due to the added NaCl. Furthermore, interfacial forces calculation showed that, for the 0.001 M NaCl solution, the presence of strong electrostatic repulsion with a positive energy barrier. Yet with the increasing amount of NaCl concentration (i.e., 0.01 and 0.1 M), there was the weakening of the electrostatic repulsion force. Uchida et al.[18] also showed a similar reduction in $\zeta$ potential with the addition of salts. Furthermore, the pressure calculation showed the reduction in the interfacial pressure difference with the increased NaCl concentration, yet the amount of the reduction is not sufficient to compensate for the pressure created due to the surface tension. The experimental results reported in this study and the application of the diffused double layer were limited to oxygen bubbles in different solutions of NaCl concentrations. The applicability of diffuse double layer theory for different solution chemistries should be investigated. Literature suggests bubble clustering to prevent gas diffusion. Also, there is a possibility of a reduction in surface tension of water due to the dissolution of salts,[64−66] which is not considered in this research. Finally, this research assumed that surface charge on bubbles consisted of $OH^-$ but was not included in any calculations. However, there is a good possibility that those negative charges may be $(HCO^3)^-$ ions due to dissolved $CO_2$ in the air. All these need to be further studied to develop a comprehensive theory for nanobubbles behavior using molecular dynamics simulations.

## ASSOCIATED CONTENT

### Supporting Information

The Supporting Information is available free of charge on the ACS Publications website at DOI: 10.1021/acs.langmuir.9b01443.

Derivation of modified Young−Laplace equation, derivation of surface charge density equation for nanobubbles and the interaction energy/forces equations (PDF)

## AUTHOR INFORMATION


### Corresponding Author

*E-mail: meegoda@njit.edu.

### ORCID

Jay N. Meegoda: 0000-0002-8406-7186
Shaini Aluthgun Hewage: 0000-0001-7767-0000
Janitha H. Batagoda: 0000-0003-2616-150X


### Notes

The authors declare no competing financial interest.

## ACKNOWLEDGMENTS

This research was sponsored by the US National Science Foundation Award 1634857 entitled "Remediation of Contaminated Sediments with Ultrasound and Ozone Nanobubbles". The program manager at NSF is Dr. Richard Fragaszy. Authors also would like to thank Professor Wen Zhang for the support in the DLS analysis.



DOI: 10.1021/acs.langmuir.9b01443
Langmuir 2019, 35, 12100−12112

## REFERENCES


(1) Agarwal, A.; Ng, W. J.; Liu, Y. Principle and applications of microbubble and nanobubble technology for water treatment. *Chemosphere* **2011**, *84* (9), 1175−1180.

(2) Berkum, V. E. Fine bubble technology is an exciting innovative technology that has potential applications for an impressive range of industries. https://www.linkedin.com/pulse/smart-people-talk-bubbles-water-innovation-erik-van-berkum/?lipi=urn%3Ali%3Apage%3Ad_flagship3_profile_view_base%3Bv4eB2KYhTCGgZRI7I2Uw4g%3D%3D (accessed January 23, 2018).

(3) Ebina, K.; Shi, K.; Hirao, M.; Hashimoto, J.; Kawato, Y.; Kaneshiro, S.; Morimoto, T.; Koizumi, K.; Yoshikawa, H. Oxygen and air nanobubble water solution promote the growth of plants, fishes, and mice. *PLoS One* **2013**, *8* (6), No. e65339.

(4) Nirmalkar, N.; Pacek, A. W.; Barigou, M. On the existence and stability of bulk nanobubbles. *Langmuir* **2018**, *34* (37), 10964−10973.

(5) Ushikubo, F. Y.; Furukawa, T.; Nakagawa, R.; Enari, M.; Makino, Y.; Kawagoe, Y.; Shiina, T.; Oshita, S. Evidence of the existence and the stability of nano-bubbles in water. *Colloids Surf., A* **2010**, *361* (1−3), 31−37.

(6) Liu, S.; Kawagoe, Y.; Makino, Y.; Oshita, S. Effects of nanobubbles on the physicochemical properties of water: The basis for peculiar properties of water containing nanobubbles. *Chem. Eng. Sci.* **2013**, *93*, 250−256.

(7) Takahashi, M. $\zeta$ potential of microbubbles in aqueous solutions: electrical properties of the gas- water interface. *J. Phys. Chem. B* **2005**, *109* (46), 21858−21864.

(8) Oh, S. H.; Kim, J. M. Generation and Stability of Bulk Nanobubbles. *Langmuir* **2017**, *33* (15), 3818−3823.

(9) Chaplin, M. Nanobubbles (ultrafine bubbles). http://www1.lsbu.ac.uk/water/nanobubble.html (accessed January 24, 2018).

(10) Sekiguchi, T.; Kawaguchi, T.; Saito, T.; Satoh, I. Investigation of Brownian Motion of Micro and Nano-Bubble [abstract]. *Nippon Kikai Gakkai Ronbunshu, B-hen* **2011**, *77* (784), 2316−2327.

(11) Ljunggren, S.; Eriksson, J. C. The lifetime of a colloid-sized gas bubble in water and the cause of the hydrophobic attraction. *Colloids Surf., A* **1997**, *129*, 151−155.

(12) German, S. R.; Chen, Q.; Edwards, M. A.; White, H. S. Electrochemical Measurement of Hydrogen and Nitrogen Nanobubble Lifetimes at Pt Nanoelectrodes. *J. Electrochem. Soc.* **2016**, *163* (4), H3160−H3166.

(13) Batagoda, J. H.; Aluthgun Hewage, S. D.; Meegoda, J. N. Nano-ozone bubbles for drinking water treatment. *J. Environ. Eng. Sci.* **2017**, *12*, 1−10.

(14) Weijs, J. H.; Seddon, J. R.; Lohse, D. Diffusive shielding stabilizes bulk nano bubble clusters. *ChemPhysChem* **2012**, *13* (8), 2197−2204.

(15) Liu, H.; Cao, G. Effectiveness of the Young-Laplace equation at nanoscale. *Sci. Rep.* **2016**, *6*, 23936.

(16) Bunkin, N. F.; Yurchenko, S. O.; Suyazov, N. V.; Shkirin, A. V. Structure of the nanobubble clusters of dissolved air in liquid media. *J. Biol. Phys.* **2012**, *38* (1), 121−152.

(17) Dressaire, E.; Bee, R.; Bell, D. C.; Lips, A.; Stone, H. A. Interfacial polygonal nano patterning of stable microbubbles. *Science* **2008**, *320* (5880), 1198−1201.

(18) Uchida, T.; Liu, S.; Enari, M.; Oshita, S.; Yamazaki, K.; Gohara, K. Effect of NaCl on the lifetime of micro-and nano bubbles. *Nanomaterials* **2016**, *6* (2), 31.

(19) Temesgen, T.; Bui, T. T.; Han, M.; Kim, T. I.; Park, H. Micro and nano bubble technologies as a new horizon for water-treatment techniques: A review. *Adv. Colloid Interface Sci.* **2017**, *246*, 40−51.

(20) Salgin, S.; Salgin, U.; Bahadir, S. Zeta potentials and isoelectric points of biomolecules: the effects of ion types and ionic strengths. *Int. J. Electrochem. Sci.* **2012**, *7* (12), 12404−12414.

(21) Liu, X.; Ding, W.; Tian, R.; Du, W.; Li, H. Position of Shear Plane at the Clay−Water Interface: Strong Polarization Effects of Counterions. *Soil Science Society of America Journal* **2017**, *81* (2), 268−276.

(22) Ding, W.; Liu, X.; Song, L.; Li, Q.; Zhu, Q.; Zhu, H.; Feinan, H.; Yaxue, L.; Longhui, Z.; Li, H. An approach to estimate the position of the shear plane for colloidal particles in an electrophoresis experiment. *Surf. Sci.* **2015**, *632*, 50−59.

(23) Sainath, K.; Ghosh, P. Electrical Properties of Silicone Oil-Water Interface in the Presence of Ionic Surfactants and Salt: Importance in the Stability of Oil-in-Water Emulsions. *Chem. Eng. Commun.* **2014**, *201* (12), 1645−1663.

(24) Li, H.; Wei, S.; Qing, C.; Yang, J. Discussion on the position of the shear plane. *J. Colloid Interface Sci.* **2003**, *258* (1), 40−44.

(25) Delgado, A. V.; González-Caballero, F.; Hunter, R. J.; Koopal, L. K.; Lyklema, J. Measurement and interpretation of electrokinetic phenomena. *J. Colloid Interface Sci.* **2007**, *309* (2), 194−224.

(26) Leroy, P.; Jougnot, D.; Revil, A.; Lassin, A.; Azaroual, M. A double layer model of the gas bubble/water interface. *J. Colloid Interface Sci.* **2012**, *388* (1), 243−256.

(27) Verwey, E. J. W.; Overbeek, J. T. G.; Overbeek, J. T. G. *Theory of the stability of lyophobic colloids*; Elsevier: Amsterdam, 1948.

(28) Tripathy, S.; Bag, R.; Thomas, H. R. Effect of Stern-layer on the compressibility behavior of bentonites. *Acta Geotechnica* **2014**, *9* (6), 1097−1109.

(29) Shang, J. Q.; Lo, K. Y.; Quigley, R. M. Quantitative determination of potential distribution in Stern−Gouy double layer model. *Can. Geotech. J.* **1994**, *31* (5), 624−636.

(30) Sridharan, A.; Satyamurty, P. V. Potential-distance relationships of clay-water systems considering the Stern theory. *Clays Clay Miner.* **1996**, *44* (4), 479−484.

(31) Brown, M. A.; Abbas, Z.; Kleibert, A.; Green, R. G.; Goel, A.; May, S.; Squires, T. M. Determination of surface potential and electrical double layer structure at the aqueous electrolyte-nanoparticle interface. *Phys. Rev. X* **2016**, *6* (1), 011007.

(32) Herbowski, L.; Gurgul, H.; Staron, W. Experimental determination of the Stern layer thickness at the interface of the human arachnoid membrane and the cerebrospinal fluid. *Z. Med. Phys.* **2009**, *19* (3), 189−192.

(33) Allison, S.; Rasmusson, M.; Wall, S. The primary electroviscous effect, free solution electrophoretic mobility, and diffusion of dilute prolate ellipsoid particles (minor axis = 3 nm) in monovalent salt solution. *J. Colloid Interface Sci.* **2003**, *258* (2), 289−297.

(34) Lim, J.; Whitcomb, J.; Boyd, J.; Varghese, J. Transient finite element analysis of electric double layer using Nernst−Planck−Poisson equations with a modified Stern layer. *J. Colloid Interface Sci.* **2007**, *305* (1), 159−174.

(35) Brown, M. A.; Goel, A.; Abbas, Z. Effect of electrolyte concentration on the Stern layer thickness at a charged interface. *Angew. Chem., Int. Ed.* **2016**, *55* (11), 3790−3794.

(36) Kielland, J. Individual activity coefficients of ions in aqueous solutions. *J. Am. Chem. Soc.* **1937**, *59* (9), 1675−1678.

(37) Debye, P.; Hückel, E. *Phys. Z.* **1923**, *24*, 742.

(38) Tuinier, R. Approximate solutions to the Poisson−Boltzmann equation in spherical and cylindrical geometry. *J. Colloid Interface Sci.* **2003**, *258* (1), 45−49.

(39) Loeb, A. L.; Overbeek, J. T. G.; Wiersema, P. H.; King, C. V. The electrical double layer around a spherical colloid particle. *J. Electrochem. Soc.* **1961**, *108* (12), 269C−269C.

(40) Ohshima, H.; Healy, T. W.; White, L. R. Accurate analytic expressions for the surface charge density/surface potential relationship and double layer potential distribution for a spherical colloidal particle. *J. Colloid Interface Sci.* **1982**, *90* (1), 17−26.

(41) Leite, F. L.; Bueno, C. C.; Da Róz, A. L.; Ziemath, E. C.; Oliveira, O. N. Theoretical models for surface forces and adhesion and their measurement using atomic force microscopy. *Int. J. Mol. Sci.* **2012**, *13* (10), 12773−12856.

(42) Uskoković, V. Dynamic light scattering based microelectrophoresis: main prospects and limitations. *J. Dispersion Sci. Technol.* **2012**, *33* (12), 1762−1786.

(43) Xie, L.; Shi, C.; Cui, X.; Zeng, H. Surface forces and interaction mechanisms of emulsion drops and gas bubbles in complex fluids. *Langmuir* **2017**, *33* (16), 3911−3925.

(44) Xie, L.; Shi, C.; Cui, X.; Huang, J.; Wang, J.; Liu, Q.; Zeng, H. Probing the interaction mechanism between air bubbles and bitumen




DOI: 10.1021/acs.langmuir.9b01443
*Langmuir* 2019, 35, 12100−12112

surfaces in aqueous media using bubble probe atomic force microscopy. *Langmuir* **2018**, *34* (3), 729−738.
(45) Chen, A.; Li, S. W.; Sang, F. N.; Zeng, H. B.; Xu, J. H. Interactions between micro-scale oil droplets in aqueous surfactant solution determined using optical tweezers. *J. Colloid Interface Sci.* **2018**, *532*, 128−135.
(46) Meegoda, J. N.; Aluthgun Hewage, S.; Batagoda, J. H. Stability of Nanobubbles. *Environmental Engineering Science* **2018**, *35* (11), 1216−1227.
(47) Fan, M.; Tao, D.; Honaker, R.; Luo, Z. Nano bubble generation and its application in froth flotation (part I): nano bubble generation and its effects on properties of microbubble and millimeter scale bubble solutions. *Min. Sci. Technol. (Xuzhou, China)* **2010**, *20* (1), 1−19.
(48) Agarwal, A.; Ng, W. J.; Liu, Y. Principle and applications of microbubble and nano bubble technology for water treatment. *Chemosphere* **2011**, *84* (9), 1175−1180.
(49) Tsuge, H., Ed. *Micro-and Nanobubbles: Fundamentals and Applications*; CRC Press, 2014.
(50) Meegoda, J. N.; Batagoda, J. H.; Aluthgun-Hewage, S. Briefing: In situ decontamination of sediments using ozone nano bubbles and ultrasound. *J. Environ. Eng. Sci.* **2017**, *12* (1), 1−3.
(51) Batagoda, J. H.; Hewage, S. D. A.; Meegoda, J. N Remediation of heavy-metal-contaminated sediments in USA using ultrasound and ozone nanobubbles. *J. Environ. Eng. Sci.* **2019**, *14*, 130−138.
(52) Zhang, M.; Seddon, J. R. Nanobubble−nanoparticle interactions in bulk solutions. *Langmuir* **2016**, *32* (43), 11280−11286.
(53) Azevedo, A.; Etchepare, R.; Calgaroto, S.; Rubio, J. Aqueous dispersions of nanobubbles: Generation, properties and features. *Miner. Eng.* **2016**, *94*, 29−37.
(54) Calgaroto, S.; Wilberg, K. Q.; Rubio, J. On the nanobubbles interfacial properties and future applications in flotation. *Miner. Eng.* **2014**, *60*, 33−40.
(55) *Zetasizernano series user manual*; Malvern Instruments, 2004.
(56) Schnitzer, O.; Frankel, I.; Yariv, E. Electrophoresis of bubbles. *J. Fluid Mech.* **2014**, *753*, 49−79.
(57) Nakashima, S.; Spiers, C. J.; Mercury, L.; Fenter, P. A.; Hochella, M. F., Jr. *Physico-chemistry of Water in Geological and Biological Systems—Structures and properties of Thin Aqueous Films*; Universal Academy Press, Inc.: Tokyo, 2004; pp 2−5.
(58) Ohgaki, K.; Khanh, N. Q.; Joden, Y.; Tsuji, A.; Nakagawa, T. Physicochemical approach to nano bubble solutions. *Chem. Eng. Sci.* **2010**, *65* (3), 1296−1300.
(59) Higuchi, S.; Satoh, M. Effects of NaCl, NaOH, and HCl concentration on the cloud point of poly (vinyl methyl ether) in water—electrostatic interactions are inevitably involved in the hydrophobic interaction. *Colloid Polym. Sci.* **2017**, *295* (9), 1511−1520.
(60) Seddon, J. R.; Lohse, D.; Ducker, W. A.; Craig, V. S. A deliberation on nano bubbles at surfaces and in bulk. *ChemPhysChem* **2012**, *13* (8), 2179−2187.
(61) Goldman, S.; Solano-Altamirano, M.; Ledez, K. Driving force of gas-bubble growth and dissolution. *Gas Bubble Dynamics in the Human Body*; Academic Press: Cambridge, MA, 2018; pp 49−62.
(62) Hu, L.; Xia, Z. Application of ozone micro-nano-bubbles to groundwater remediation. *J. Hazard. Mater.* **2018**, *342*, 446−453.
(63) Cho, S. H.; Kim, J. Y.; Chun, J. H.; Kim, J. D. Ultrasonic formation of nanobubbles and their zeta-potentials in aqueous electrolyte and surfactant solutions. *Colloids Surf., A* **2005**, *269* (1), 28−34.
(64) Jones, G.; Ray, W. A. The surface tension of solutions of electrolytes as a function of the concentration. I. A differential method for measuring relative surface tension. *J. Am. Chem. Soc.* **1937**, *59* (1), 187−198.
(65) Jones, G.; Ray, W. A. The surface tension of solutions of electrolytes as a function of the concentration II. *J. Am. Chem. Soc.* **1941**, *63* (1), 288−294.
(66) Duignan, T.; Baer, M.; Mundy, C. Surfactant Impurities Can Explain the Jones-Ray Effect. **2018**, *ChemRxiv:5732976.v3*. chemrxiv.org preprint archive. https://chemrxiv.org/articles/Surfactant_Impurities_Can_Explain_the_Jones-Ray_Effect/5732976/3 (accessed May 15, **2019**).



DOI: 10.1021/acs.langmuir.9b01443
*Langmuir* 2019, 35, 12100−12112